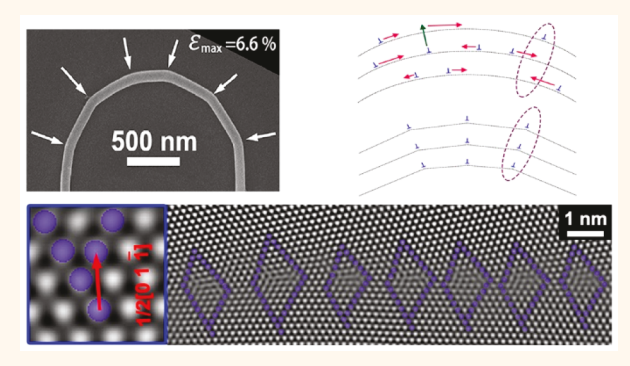
Strain-Energy Release in Bent Semiconductor Nanowires Occurring by Polygonization or **Nanocrack Formation**

Zhiyuan Sun, †© Chunyi Huang, † Jinglong Guo, ‡ Jason T. Dong, † Robert F. Klie, ‡ Lincoln J. Lauhon, *, †© and David N. Seidman*,†,§

Supporting Information

Downloaded via UNIV OF ILLINOIS CHICAGO on September 27, 2019 at 20:59:27 (UTC). See https://pubs.acs.org/sharingguidelines for options on how to legitimately share published articles.

ABSTRACT: Strain engineering of semiconductors is used to modulate carrier mobility, tune the energy bandgap, and drive growth of self-assembled nanostructures. Understanding strainenergy relaxation mechanisms including phase transformations, dislocation nucleation and migration, and fracturing is essential to both exploit this degree of freedom and avoid degradation of carrier lifetime and mobility, particularly in prestrained electronic devices and flexible electronics that undergo large changes in strain during operation. Raman spectroscopy, highresolution transmission electron microscopy, and electron diffraction are utilized to identify strain-energy release mechanisms of bent diamond-cubic silicon (Si) and zincblende GaAs nanowires, which were elastically strained to >6%



at room temperature and then annealed at an elevated temperature to activate relaxation mechanisms. High-temperature annealing of bent Si-nanowires leads to the nucleation, glide, and climb of dislocations, which align themselves to form grain boundaries, thereby reducing the strain energy. Herein, Si nanowires are reported to undergo polygonization, which is the formation of polygonal-shaped grains separated by grain boundaries consisting of aligned edge dislocations. Furthermore, strain is shown to drive dopant diffusion. In contrast to the behavior of Si, GaAs nanowires release strain energy by forming nanocracks in regions of tensile strain due to the weakening of As-bonds. These insights into the relaxation behavior of highly strained crystals can inform the design of nanoelectronic devices and provide guidance on mitigating degradation.

KEYWORDS: nanowire, strain, polygonization, nanocrack, plastic deformation, dislocation

lastic strain is used to modulate the bandgap and charge carrier mobility of semiconducting crystals, providing an important degree-of-freedom in semiconductor device engineering. Plastic deformation, or the nucleation and migration of dislocations to relieve strain, must concurrently be controlled to avoid electronic device degradation and failure.^{2,3} Dislocation nucleation and migration are activated by strain and temperature, leading to thresholds for plastic relaxation specific to the device geometry and operating conditions. For example, in highly scaled fieldeffect transistors (FET), such as Fin-FETs with strained channels, high operating temperatures can activate dislocation nucleation, which degrades charge mobilities, reduces the threshold voltage, and increases the leakage current.4

Flexible electronic devices must survive hundreds of thousands of cycles without fatigue and/or creep, which could result from strain-activated dislocation nucleation and migration. Because relaxations leading to degradation originate at the atomic scale, a nanoscopic understanding of relaxation mechanisms is essential to the engineering of reliable electronic and photonic devices.

Intriguingly, single-crystal semiconductor nanowires represent an exciting platform for the development of nanoelectric

Received: February 13, 2019 Accepted: February 26, 2019 Published: February 26, 2019

Department of Materials Science and Engineering, Northwestern University, 2220 Campus Drive, Evanston, Illinois 60208-3108, United States

^{*}Department of Physics, University of Illinois at Chicago, Chicago, Illinois 60607, United States

[§]Center for Atom-Probe Tomography (NUCAPT), Northwestern University, 2220 Campus Drive, Evanston, Illinois 60208-3108, United States

devices⁸ and exploration of the nanoscale origins of mechanical properties.⁹ Due to the perfection of the interiors and surfaces of nanowires, their elastic properties approach theoretical predictions, making them excellent candidates for fundamental studies of the onset of dislocation nucleation and fracture upon tensile stretching and bending.^{10–14} In the absence of pre-existing defects, which may decrease nucleation barriers of additional defects, semiconductor nanowires, including Si and GaAs, can tolerate large elastic deformation without plasticity or fracture in tension¹⁴ and/or bending^{11,15} at room temperature. This suggests that they may also be more resistant to degradation in some device contexts. In contrast, plasticity is readily observed in ductile metal nanowires, such as Au and Pd, in which dislocations nucleate at the surface upon bending.^{10,16,17}

Advances in microelectromechanical systems (MEMS) testing stages and in situ transmission/scanning electron microscopy (T/SEM) have enabled many important studies of the mechanical properties of nanowires. 14,18,19 It is, however, emphasized that even brittle semiconductors may display plasticity under electron-beam illumination, which facilitates the nucleation and migration of dislocations. 17,20 While studies that observe extrinsic plasticity²¹ are numerous, there have been far fewer investigations of thermally activated intrinsic plasticity of nanowires, which are completely free of measurement artifacts. Thermal annealing of strained nanowires, with observations before and after annealing, can be used to explore the metastable quasi-equilibrium configurations of imperfections in nanowires that relieve strain. The thresholds for dislocation nucleation and migration in nanoscale single-crystals based on experiments better represent the possible performance limits of these materials.

Herein, we report analyses of strain relaxation mechanisms in bent Si and GaAs nanowires, subjected to high-temperature annealing to explore fundamental thresholds for plastic relaxation. The nanowires are maintained in bent configurations on flat substrates and then annealed at a high temperature to activate relaxation mechanisms that are inaccessible at room temperature. Silicon nanowires transform from continuously bent single crystals to discrete polygonal grains following the nucleation and strain-driven alignment of edge dislocations into periodic grain boundaries. Strain also drives the diffusion of P and B dopant atoms, providing an additional relaxation mechanism. Polygonization was first observed in 1949²² by bending and annealing macroscopic crystals of iron-silicon, ²³ Zn, ²⁴ GaAsP, ²⁵ Si, ²⁶ or NaCl, ²⁷ at an elevated temperature. At elevated temperatures, dislocations generated by the bending strain can rearrange themselves endto-end by a combination of glide and climb mechanisms. While polygonization has been observed in a metal nanowire, ²⁸ it has not been reported for brittle semiconductor nanowires. Additionally, we find that bent GaAs nanowires do not polygonize as a result of dislocation glide and climb. Instead, they exhibit a mixture of plastic and brittle behavior as they relax into polygonal morphologies resulting from the formation of nanoscale cracks propagating from the nanowire's surfaces under tensile strain. Both relaxation modalities reveal ways to release the bending strain energy in semiconductor nanowires at elevated temperatures.

RESULTS AND DISCUSSION

Silicon nanowires grown using a gold droplet mediated vaporliquid-solid process (see Experimental Methods) were transferred to native-oxide-coated Si substrates to generate regions of compressive and tensile strains, varying from 0 to 7% (Figure 1). Electron backscatter diffraction (EBSD)

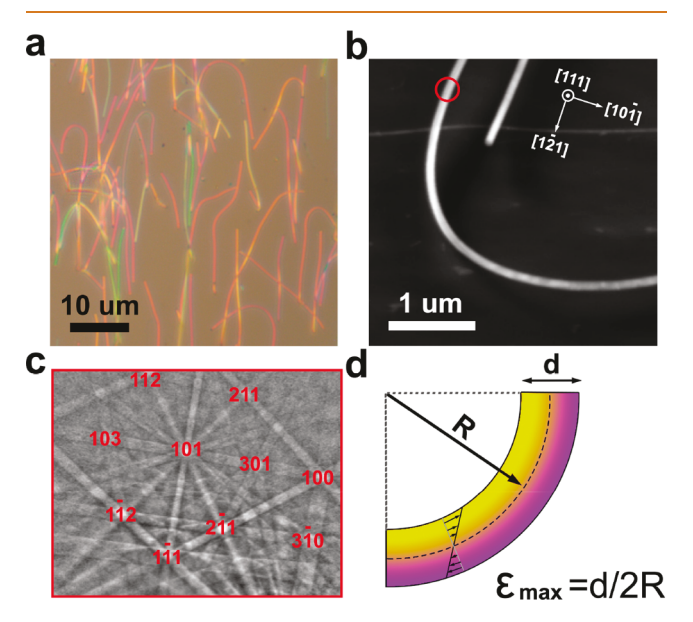


Figure 1. Mechanical transfer creates continuously varying strain in Si nanowires. (a) Optical microscope image of bent Si nanowires. (b) SEM micrograph of a bent Si nanowire. (c) EBSD pattern taken from the region indicated by the red circle in (b), which is utilized to determine the nanowire's growth direction and out-of-plane direction. (d) Schematic diagram of the elastic strain profile generated by bending, where the maximum tensile (compressive) strain at the outer (inner) surface is given by d/2R, where d is the nanowire's diameter and R is the bending radius; the black dashed curve is the so-called neutral plane, which is well known from linear elasticity theory of the bending of macroscopic beams.

analyses of 31 nanowires with average diameters of 100 nm demonstrated that the nanowires are $\langle 112 \rangle$ -oriented bicrystals with $\{111\}$ planes parallel to the substrate (Figure 1b, Figure S1) due to the dimensions of the two $\{111\}$ facets on opposite sides of a Si nanowire. At room temperature, the deformation mode is anticipated to be elastic for the range of strains examined in this study. The outer surface of the bent region is under tensile strain, while the inside region is under compressive strain, with the maximum strain given by d/2R, where d is the nanowire's diameter and R is the bending radius according to the Euler—Bernoulli elastic theory of the bending of beams (Figure 1d). The magnitude of the strain decreases linearly toward the center of the Si nanowire, which is the so-called neutral plane of the bent Si nanowire.

Correlated Raman microscopy and scanning electron microscopy (SEM) were utilized to map the elastic strain distribution at room temperature and observe strain relaxation activated by annealing at an elevated temperature (Figure 2). Toward this end, bent nanowires were annealed in 5% H_2 (balance N_2) at 920 °C for 4 min with the expectation that dislocations will be nucleated at a nanowire's surface 10,21 and migrate 30 under the influence of the strain gradients created by bending and dislocation-dislocation interactions. Prior to annealing, imaging of a Si nanowire's Raman scattering intensity (Figure 2a) and the full-width at half-maximum (fwhm) (Figure 2b) confirmed that the peak elastic strain occurs at the position of the maximum bending radius (Figure

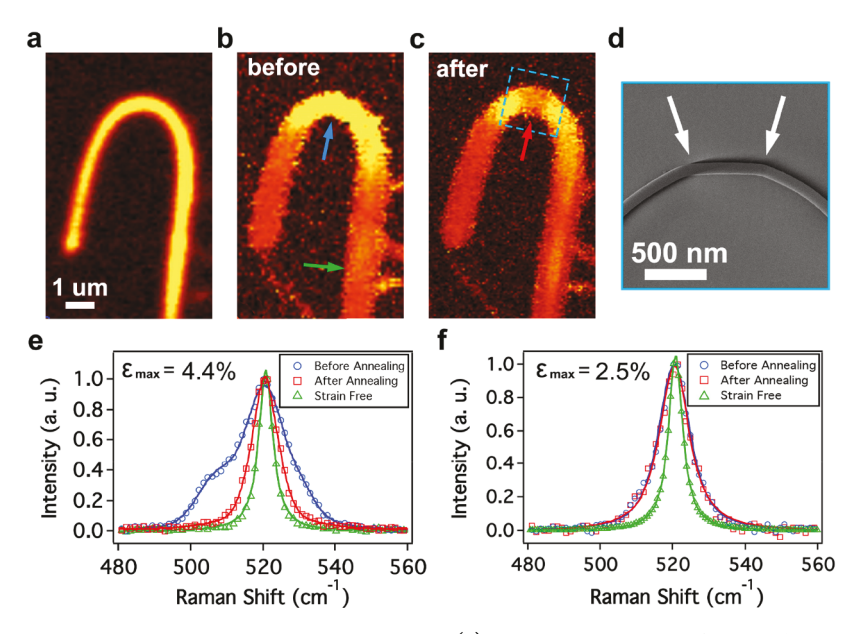


Figure 2. Analysis of elastic strain variations using Raman spectroscopy. (a) Integrated intensity of F_{2g} mode at 519 cm⁻¹, prior to annealing the nanowire to a maximum strain of 4.4%. (b, c) Map of fwhm of F_{2g} mode before (b) and after (c) thermal annealing. (d) SEM image of a bent region indicated by the blue square in (c); white arrows indicate the positions of the polygonization walls, which are grain boundaries consisting of edge dislocations. (e) Raman spectra of strain-free region (green), region of 4.4% strain before annealing (blue), and the strained region after annealing (green). The blue and red colored arrows in (b) and (c) indicate the locations where Raman spectra were acquired. (f) Raman spectra before and after annealing the nanowire with a maximum strain of 2.5%; note that relaxation is not observed.

2b, blue arrow); the tensile and compressive strains in the inner and outer bending surfaces produce opposite peak shifts of the F_{2g} mode, leading to an overall increase in the fwhm values in the strained regions of the nanowire (Figure 2e,f).³ For nanowires above a critical strain threshold of 3%, discussed further below, annealing to 920 °C reduces the fwhm values (Figure 2e) preferentially at the position of maximum bending strain (Figure 2c, red arrow). This implies a reduction in the elastic strain and concomitantly the elastic strain energy, within the region sampled by the confocal Raman measurement (~500 nm fwhm); that is, the elastic strain energy has been relaxed. In these regions, we also observe microscopic bending in the form of abrupt changes in direction in the SEM images (Figure 2d). The abrupt bends correspond to grain boundaries that consist of edge dislocations. In contrast, for a nanowire below a critical strain threshold, no change in the Raman fwhm is observed (Figure 2f), and its morphology is unchanged. As demonstrated below, annealing of highly strained Si nanowires leads to relaxation of the elastic strain energy through plastic deformation, which involves the nucleation of edge dislocations. Furthermore, the global strain energy in the bent region is reduced as a result of polygonization,³² which has not heretofore been reported in semiconductor nanowires.

At elevated temperatures, the stress in the bent region drives collective dislocation motion, which leads to polygonization or the formation of discrete crystalline grains joined by grain boundaries consisting of aligned and regularly spaced edge dislocations (Figure 3, Figure S2). High-angle annular dark-field (HAADF) STEM imaging establishes that edge dislocations with [110]-type Burgers vectors align with approximately equal spacing to form low-angle (<10°) grain boundaries (Figure 3c-f), which are visible as abrupt changes in the nanowire axis in the SEM images. Images of high-angle (>20°) grain boundaries are presented in the Figure S3. The bright contrast effects surrounding the edge dislocations indicates segregation of Au atoms, which are incorporated in

the nanowire from the Au catalyst during VLS growth, 33,34 to the tilt grain boundaries, forming Cottrell atmospheres 35 (Figure 3c,d; Figure S4). Both $1/2[\overline{1}\ 1\ 0]$ and $1/2[0\ 1\ \overline{1}]$ dislocations are observed (Figure 3d,e). A grain boundary can be composed of both types of edge-dislocations (Figure 3c) or only one type of edge-dislocation (Figure 3f). The dislocation spacing D at tilt or twist boundaries can be calculated from the Read—Shockley equation, which is applicable for either a symmetric tilt or twist grain boundary for any value of θ :

$$D = \frac{b}{2} / (\sin(\theta/2)) \tag{1}$$

where b = 0.383 nm, the magnitude of the $1/2[0\ 1\ 1]$ Burger's vector, and θ is the tilt angle (radian), which is 11.1° (0.19 rad) for the tilt boundary in Figure 3f. The calculated interdislocation spacing, 1.98 nm, is very close to that measured value utilizing a HRTEM image, 2.03 nm.

The process of polygonization proceeds sequentially through three steps: (1) [1 1 0] edge dislocations identified in Figure 3 are generated at the surface of the nanowire; 21 (2) the edge dislocations glide on {1 1 2}-type slip planes; and (3) the edgedislocations climb normal to {1 1 2}-type slip planes and align themselves in dislocation arrays to form symmetric tilt grain boundaries. 12 In polygonization, the climb of edge dislocations is the rate-limiting step; climb involves nonconservative motion of an edge dislocation because it requires mass transport mediated by thermally activated vacancy migration, and the activation energy for migration of a vacancy³⁶⁻³⁸ exceeds that of nucleation. Polygonization by edge dislocation climb has been observed previously in macroscopic Ge crystals subjected to the same bending strain geometry as used herein.³⁹ A more detailed study on iron-silicon specimens demonstrated that edge dislocations form and slip at relatively low-temperatures (600 °C), whereas polygonization occurs only at a higher temperature once thermally activated dislocation climb occurs. 23 Although polygonization has been

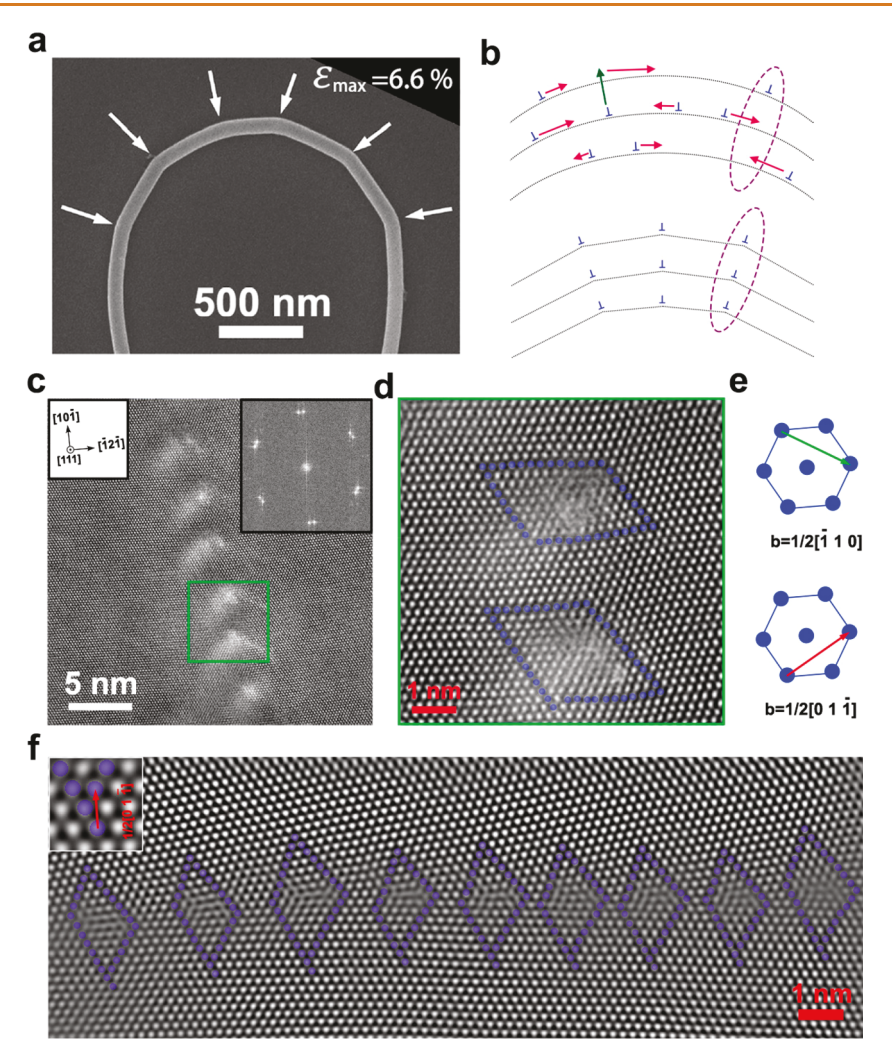


Figure 3. (a) A polygonized Si nanowire with six tilt grain boundaries indicated by white arrows. (b) Schematic diagrams of edge dislocations formed by annealing, which involve both glide (red arrow) and climb (green arrow) processes to form symmetric tilt grain boundaries between the straight segments. (c) HAADF STEM image of a symmetric tilt grain boundary. Inset: fast Fourier transform of image in (c) indicating the $\begin{bmatrix} 1 & 1 & 1 \end{bmatrix}$ zone-axis and crystal rotation at the bend. (d) Edge dislocations from the green box in (c). Blue dots indicate a Burgers circuit identifying the edge dislocations shown in (e) green arrow $1/2\begin{bmatrix} 1 & 1 & 0 \end{bmatrix}$, red arrow $1/2\begin{bmatrix} 0 & 1 & 1 \end{bmatrix}$. (f) Array of $\begin{bmatrix} 0 & 1 & 1 \end{bmatrix}$ edge dislocations at a symmetric tilt grain boundary.

observed in bulk specimens, it is worth noting differences in dislocation nucleation and motion between bulk Si and Si nanowires. First, because nanowires are single crystals, the surface is the source of dislocations, which form more easily at the surface due a reduced activation energy; the large surfaceto-volume ratio of Si nanowires implies that dislocation generation per unit volume is greater in nanowires than bulk in Si. Second, the small nanowire diameter (~100 nm) implies that polygonization can occur with rather short glide and climb distances compared to bulk specimens, and therefore faster. In summary, polygonization is kinetically more favorable in nanowires. A more extensive discussion of polygonization in bulk Si is found elsewhere. 40 Herein, we consider how the activated nature of dislocation nucleation, glide, and climb leads to the observation of a threshold strain for polygonization of a nanowire, analyzed using Raman spectroscopy studies as described below.

Dislocation nucleation is a thermally activated process occurring at a rate, ν , that is modeled using the following equations: 41,42

$$\nu = N\nu_0 \exp\left(-\frac{\Delta G_{\text{act}}(\sigma, T)}{k_{\text{B}}T}\right)$$
 (2)

and

$$\Delta G_{\text{act}}(\sigma, T) = \Delta U_{\text{act}} \left(1 - \frac{T}{T_{\text{m}}} \right) \left(1 - \frac{\sigma}{\sigma_{\text{ath}}} \right)^{\alpha}$$
(3)

where T is the sample temperature in Kelvin, $T_{\rm m}$ is the melting temperature in Kelvin, σ is the stress in the direction along which the dislocation forms, $\sigma_{\rm ath}$ is the athermal strength (a constant), $\Delta U_{\rm act}$ is the nucleation barrier at zero Kelvin and zero strain, N is the number of equivalent nucleation sites, ν_0 is an attempt frequency for crossing the nucleation barrier, and α is a material-dependent constant. Dislocation formation occurs preferentially at regions of high stress due to a lowering of the nucleation barrier as modeled by eq 3. A detailed study of Si nanowires demonstrates that the type of dislocation (perfect or partial) and the region of nucleation (tensile or compressive region) depends on the sign and magnitude of the strain. The yield point is the strain below which dislocation

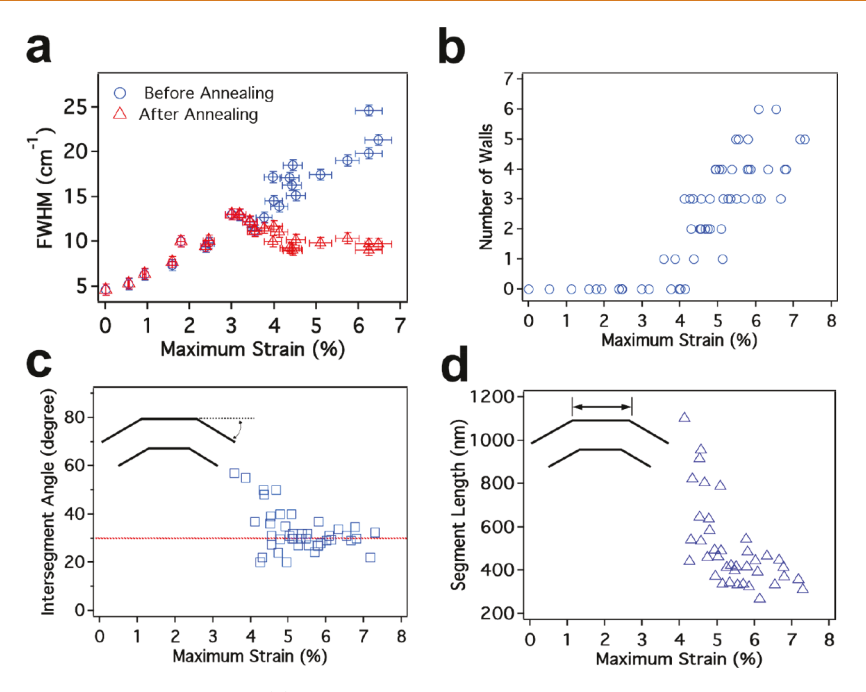


Figure 4. Impact of peak strain on polygonization. (a) Raman peak fwhm between the polygonally shaped grains before (blue) and after (red) thermal annealing for 24 nanowires with maximum strain values ranging from 0 to 7%. (b-d) The number of polygonal walls, the angles between the polygonal grains, and polygonal segment lengths as a function of the maximum strain values observed before annealing, respectively. The typical segment length of 100 nm is 4 times the diameter of the nanowire or 400 nm.

nucleation is not observed, and the yield point stress decreases with increasing temperature. For the annealing temperature of 920 °C in this study, plastic relaxation clearly occurs in regions where the initial elastic strain is greater than or equal to ~3% as measured by decreases in the Raman mode's fwhm (Figure 2e and Figure 4a). Hence, the yield point for Si nanowires is less than or equal to 3% at 920 °C. Observations of 24 nanowires demonstrated that the Si peak width increases linearly as a function of the maximum strain value prior to annealing (Figure 4a, blue symbols), consistent with approximately linearly increasing elastic strain (compressive or tensile). Upon annealing, plastic relaxation reduces the fwhm in regions of >3% strain (Figure 4a, red symbols), providing evidence for plastic deformation with a strain threshold related to the formation of dislocations.

Between 3.0 and 4.5% strain, the degree of strain relaxation increases with the initial strain, confirming the role of strain in nucleation of dislocations and their migration, which leads to relaxation through polygonization. Above 4.5% strain, the Raman spectra's fwhm values achieve plateaus, and no further strain relaxation is observed. This can be explained by first observing that the angle between grain boundaries reaches a constant value of $\sim 30^{\circ}$ (Figure 4c), while the average grain's length achieves a plateau length at ~400 nm, which is four times the nanowire diameter (Figure 4d). The confocal Raman measurement, with a spatial fwhm value of ~500 nm, samples both the relaxed region and the grain boundary region in which the dislocation arrays produce elastic strain fields. 43 Hence, the Raman spectra's fwhm no longer changes as a function of the initial strain. The plateau in the angle between grain boundaries (Figure 4c) and their length (Figure 4d) also indicates that the final nanowire state is metastable, where relaxation is limited by the distance over which dislocations can climb during annealing. In principle, two small-angle grain boundaries can coalesce to form a single grain boundary with a

lower grain boundary energy than two small-angle grain boundaries. 44 Indeed, while the polygonization angle initially increases as a function of time due to grain boundary coalescence, it eventually ceases to increase due limits on dislocation climb, 23,24 which is consistent with our observations of plateaus in the angle and length of a grain boundary. The velocity of dislocation climb can be modeled as 45

The velocity of dislocation claim be inoucled as

$$r_{\rm climb} \propto \frac{\sigma}{T} D_0 \exp\left(-\frac{\Delta G_{\rm diff}}{kT}\right)$$
 (4)

where T is the sample temperature in Kelvin, σ is stress, $\Delta G_{ ext{diff}}$ is the vacancy migration activation energy, and D_0 is the preexponential factor of the expression for the diffusivity of a vacancy at room temperature. Similar to other plastic deformation and creep processes, dislocation climb is the rate-controlling step for polygonization, because dislocationclimb requires diffusion of vacancies in Si, which has a higher activation energy than does dislocation glide. 46,47 At a lower temperature or a lower stress state, the climb process is less likely to occur.⁴⁷ As with dislocation nucleation, there is a stress (strain) threshold below which the climb velocity is negligible at given temperature and therefore polygonization cannot occur. Observation of 55 Si nanowires with different strain (stress) levels indicates a strain threshold of between 3.5 and 4% (Figure 4b) for polygonization, which is greater than the dislocation nucleation threshold value of 3% (Figure 4a), as anticipated. Once the initial strain (stress) is partially relaxed to produce an angle of 30° between the ~400 nm long polygonal segments, the driving force for dislocation climb is insufficient to promote further coalescence of the polygonally shaped grains. Additionally, the interfacial strain between the Si nanowire and the Si substrate, which is not quantified herein, may also play a role in determining the precise values of the observable parameters, including the threshold for plastic

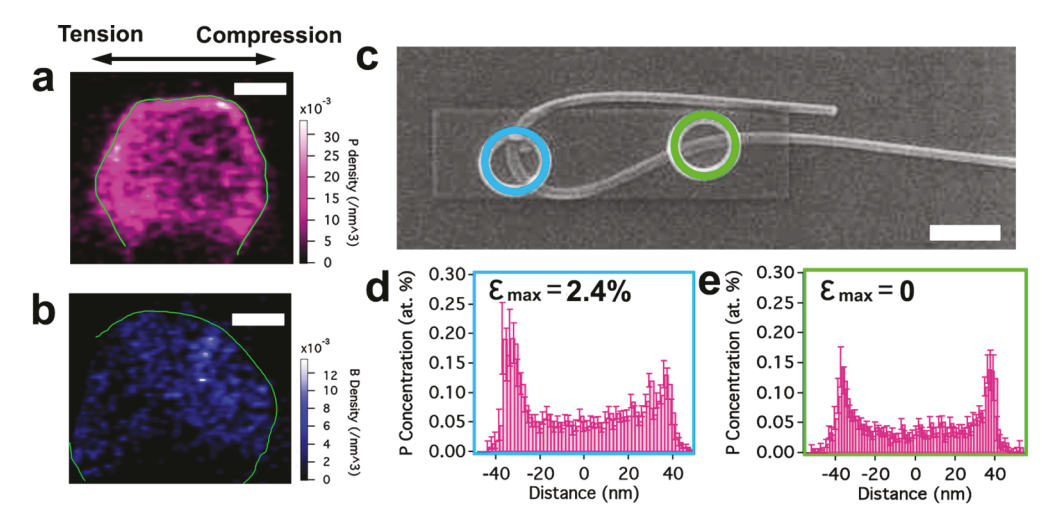


Figure 5. Redistribution of dopants in a strained Si nanowire. (a, b) Distributions of P and B dopants, respectively, in cross sections of bent Si nanowires after thermal annealing, where P or B is enriched at the tensile or compressive side, respectively; scale bar = 25 nm. The solid green lines correspond to 80 atomic % Si isoconcentration surfaces, which indicate the surface of the nanowire. (c) An SEM image of a bent P-doped Si nanowire. Scale bar is 2 μ m. (d, e) Radial P dopant profiles from strained (d) and unstrained (e) regions in (c), as indicated by the blue and green colored circles.

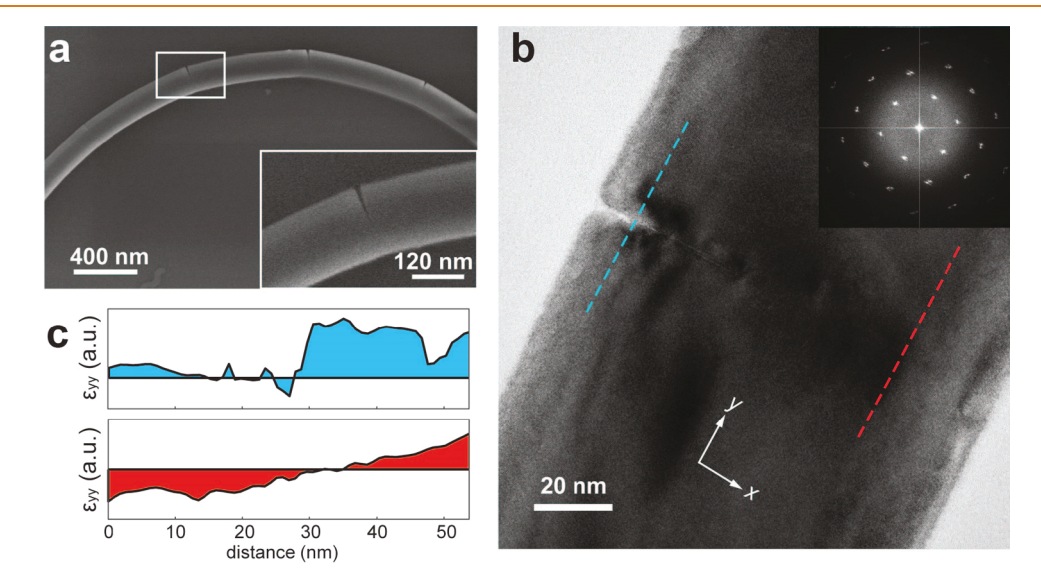


Figure 6. (a) SEM image of a bent GaAs nanowire annealed for 1 h at 450 °C. The inset figure displays a high-magnification SEM image indicated by the white rectangle. (b) TEM image of a bent and annealed GaAs nanowire. Inset: FFT of the image in (a) indicating both crystal rotation and strain relief at the crack. (c) A 10 nm-wide averaged line scan along the blue and red dashed lines in (b) displaying ε_{yy} variations in blue along the outer (top) and inner (bottom) radii in red of the nanowire. The scan direction is from the top-to-the-bottom of each line.

relaxation and the average angles between the polygonal grains and their lengths.

Although the Raman spectra do not exhibit any evidence of irreversible relaxation *via* dislocation formation below 3% strain, following annealing at 920 °C, additional activated processes could affect the nanowire structure. Specifically, density functional theory calculations have demonstrated that dopant solubility is modified by strain depending on both the dopant atom's size and charge states: In Si, small negatively charged dopant atoms, like boron (B), are more soluble under compressive strain, while large positively charged dopant atoms, like phosphorus (P), are more soluble under tensile strain. We, therefore, anticipate that under the non-uniform strain profile present in a bent nanowire, dopant atoms will be driven to the location with the highest solubility

if their diffusion is thermally activated. Atom-probe tomography (APT) with atomic ppm level chemical sensitivity was employed to analyze dopant redistribution in bent B-doped or P-doped Si nanowires (see Experimental Methods). Figure 5a,b displays the cross-sectional P and B distributions, respectively, after bending and annealing. In addition to the anticipated P segregation at the Si/SiO₂ interface, the P concentration is greater on the side of the nanowire subjected to tensile strain. Correspondingly, the B concentration is greater in the region under compressive strain. As a control, APT analyses were performed of both the strained (Figure 5d) and unstrained (Figure 5e) regions of the same nanowire (Figure 5c). The region without external strain has a symmetric P distribution, while the bent region shows an enhanced P concentration on the side under tensile strain,

which displays an unsymmetrical P segregation pattern. We note that the maximum strain in the nanowire displayed in Figure 5c is 2.4%, which is below the threshold for dislocation nucleation, \sim 3%. That implies that dopant diffusion could provide an alternative strain release mechanism at strain levels below the threshold for dislocation nucleation.

The distinct relaxation behavior of elastically strained GaAs nanowires provides an informative contrast to the case of polygonization in Si nanowires. (111)-oriented GaAs (zincblende structure) nanowires grown by a Ga-droplet seeded process (see Experimental Methods) were elastically strained at room temperature following the same procedures used for Si nanowires. They were then annealed in vacuum for 1 h at temperatures between 380 and 550 °C, which is above the brittle-to-ductile transition temperature, about 310 °C.52 Surprisingly, GaAs nanowires bent to strains of up to 6% and vacuum annealed for 1 h at 380 °C exhibited no evidence of polygonization (Supporting Information Figure S5a); apparently, this temperature is not high enough to activate dislocation climb, which motivated annealing at higher temperatures. Upon annealing at 550 °C, nanoscale pits form on the surface of unstrained nanowires due to the congruent evaporation of Ga and As atoms, 53-55 and cracks form in bent nanowires in the regions of tensile strain (Figure S5b). Annealing at an intermediate temperature of 450 °C avoids pitting in unstrained regions, but nevertheless produces cracks at regular intervals in regions of tensile strain (Figure 6a, Figure S5c), thereby demonstrating an alternative strain relief mechanism to polygonization. As with the Si nanowires, there is a strain threshold (\sim 3%) above which relaxation is activated (Figure S5d); the fact that cracks are only observed in regions of tensile strain above a threshold strain indicates that surface decomposition (leading to pitting and crack formation) is also strain activated; that is, the covalent bonds have been weakened. Furthermore, decreases in the fwhm values of the Raman spectra are not observed below ~3% strain (Figure S6), providing further evidence for an activated process. The above discussion assumes that the observed behavior patterns are not dominated by pre-existing defects; the regular spacing of cracks supports this claim.

Based on the SEM observations above and prior studies of the brittle-to-ductile transition temperature, we conclude that the mobility of dislocations in (111)-oriented GaAs nanowires is insufficient to produce polygonization prior to decomposition of GaAs, perhaps due in part to the high surface-area to volume-ratio. Instead, a crack forms at a nanowire's surface, enabling the crystal to relieve strain energy through crack formation accompanied by crystal rotation and slip with respect to the substrate. To confirm this hypothesis, HRTEM imaging was performed on bent and annealed GaAs nanowires (Figure 6b). The crystal rotation and strain relief along the nanowire's long axis are qualitatively observed in shifts of the (2 2 2) Bragg reflection in the fast-Fourier transform (FFT) pattern. Using geometric phase analyses, changes in ε_{vv} along the outer- and inner-radii were extracted, Figure 6c, top and bottom, respectively. We observe a discrete change along the outer radius, reflecting relaxation of both tensile strain and crystal rotation. In contrast, the strain variation along the inner radius is continuous, as the crystal remains continuous. Further analysis of selected areas of the nanowire is displayed in Figure S7. There are two likely reasons why the crack does not bisect the entire nanowire. First, the interface with the substrate resists slip of the nanowire; this is evident from the initial

bending strain fixed by the substrate in these experiments. Second, the formation of dislocations at the tip of a crack may cause an accumulation of compressive strain that impedes its further motion. The variations in contrast in HRTEM images are consistent with this interpretation, but detailed analysis of the dislocation structure is beyond the scope of this research. We note that the polygonization observed in Si nanowires is also enabled by translation of the nanowire with respect to the substrate, that is, slip.

CONCLUSION

In summary, we have investigated strain-energy release mechanisms in Si and GaAs nanowires by annealing bent, elastically strained nanowires supported by rigid substrates. We find that Si nanowires reduce their strain energy by polygonization due to the nucleation, slip, and climb of (110)-type dislocations. Polygonization, traditionally studied in bulk metals and semiconductors, is reported in nanowires. Combined SEM and Raman microspectroscopy studies identify a threshold strain for plastic relaxation, consistent with the thermally activated nature of the nucleation of dislocations and their migration. Polygonization is not observed below a strain of 3.5%, which is the yield point of Si at 920 °C. In contrast to Si nanowires, bent GaAs nanowires release their strain energy by forming regularly spaced cracks in regions of tensile strain due to the greater rate of strainactivated decomposition of GaAs relative to dislocation climb. Importantly, the final structure is also polygonally shaped, demonstrating that the global strain-energy relaxation mechanism in Si and GaAs is qualitatively similar, while the local relaxation mechanisms associated with the polygonal walls in Si and cracks in GaAs are distinctly different physical phenomena. Our findings may be used to analyze likely failure modes and define reliable operating regimes for nanoscale flexible electronic devices. These strain-energy relief mechanisms may also be used to fabricate new geometries of semiconducting nanostructures, such as geometric junctions with fixed angles defined by the crystallography and dislocation structure of the semiconductor itself.

EXPERIMENTAL METHODS

Nanowire Growth. Silicon nanowires were grown via vapor—liquid—solid (VLS) mechanism by a chemical vapor deposition (CVD). Au nanoparticles 50–100 nm diameter were used as the catalysts. Before nanowire growth, commercial Au colloid solution was diluted by 5 times with water and deposited onto a Si (100) substrate precoated with poly-L-lysine. The substrate was then transferred to our CVD chamber and annealed in $\rm H_2$ at 460 °C for 10 min. The nanowires were synthesized at 450–460 °C and at a total pressure of 40 Torr using SiH₄ as the Si precursor, $\rm H_2$ as the carrier gas and PH₃ (200 ppm in He)/B₂H₆ (100 ppm in He) as doping precursors. The n-type nanowires were synthesized at 460 °C with SiH₄, PH₃, and H₂ flow rate of 1, 20, and 60 sccm. The p-type nanowires were synthesized at 450 °C with SiH₄, B₂H₆, and H₂ flow rate of 2, 5, and 100 sccm. The intrinsic nanowires were synthesized at 460 °C with SiH₄ and H₂ flow rate of 2 and 100 sccm.

Transmission Electron Microscopy (TEM). The atomic resolution Z-contrast images and energy dispersive X-ray spectroscopy (EDS) mappings of polygonized Si nanowires (shown in Figure 3c,d,f) were collected using a JEOL ARM200CF aberration-corrected scanning transmission electron microscopy (STEM) operated at an accelerating voltage of 200 kV. The instrument is equipped with a cold-field emission gun and a probe spherical-aberration corrector, which permits better than 80 pm spatial resolution under optimal operating conditions. The Z-contrast images were acquired using a

high-angle annular dark-field (HAADF) detector with a collection angle variable from 90 to 175 mrad. The probe convergence semiangle was set to 29 mrad. High-resolution transmission electron microscopy (HR-TEM) images of bent GaAs nanowires with nanocracks (shown in Figure 4b) were taken along [1 1 1] zone axis using JEOL ARM300F transmission electron microscope, operated at 300 kV. Geometric phase analysis around the crack of GaAs nanowire was performed using the GPA plug-in for Digital-Micrograph.

Atom Probe Tomography (APT). To prepare APT sample, the strained nanowires on a flat substrate were coated with 80 nm zinc oxide via atomic layer deposition (ALD) first. Then the nanowire together with the coating and the substrate was lift-out in a FEI Helios dual-beam focused ion beam (FIB) with micromanipulator system and welded onto a commercial Si micropost. Finally, ion-beam annular milling was carried out to remove extra materials to get a needle-shape tip with around 100 nm diameter. APT was performed on a local-electrode atom-probe (LEAP) 4000X Si from CAMECA at 35 K and background pressure of 3.5×10^{-11} Torr. The evaporation of the specimen is controlled by a pulsed 355 nm ultraviolent focused laser at the rate of 1-1.5 ions every 100 pluses. The laser energy is set to be 25 pJ at a pulse rate of 250–500 k Hz. The APT data were reconstructed by the program IVAS 3.6.12 (CAMECA, Madison, WI) to reproduce the shape of the nanowire.

ASSOCIATED CONTENT

S Supporting Information

The Supporting Information is available free of charge on the ACS Publications website at DOI: 10.1021/acsnano.9b01231.

Additional EBSD analysis of Si nanowire orientation; SEM and TEM analysis of additional strained Si and GaAs nanowires; EDS analysis of Si nanowire at grain boundary; Raman spectroscopy of bent GaAs nanowire (PDF)

AUTHOR INFORMATION

Corresponding Authors

*E-mail: lauhon@northwestern.edu. *E-mail: d-seidman@northwestern.edu.

ORCID ®

Zhiyuan Sun: 0000-0003-3981-9083 Lincoln J. Lauhon: 0000-0001-6046-3304

Notes

The authors declare no competing financial interest.

ACKNOWLEDGMENTS

D.N.S, L.J.L., and Z.S acknowledge partial support from the United States-Israel Binational Science Foundation (grant number 2012088) and Northwestern University's McCormick School of Engineering and Applied Science. Z.S. and L.J.L. acknowledge support of DMR-1611341. The work on Si nanowires by J.G. and R.F.K was supported by the U.S. Department of Energy through EERE-SETO (DE-EE0007545) program. The acquisition of the JEOL JEM-ARM200CF at the University of Illinois at Chicago was supported by grants from the national Science Foundation (grant number DMR-0959470 and DMR-1626065). Atomprobe tomography was performed at the Northwestern University Center for Atom-Probe Tomography (NUCAPT). The LEAP tomography at NUCAPT was purchased and upgraded with grants from the NSF-MRI (DMR-0420532) and ONR-DURIP (N00014-0400798, N00014-0610539, N00014-0910781, N00014-1712870) programs. NUCAPT received support from the MRSEC program (NSF DMR-

1720139) at the Materials Research Center, the SHyNE Resource (NSF ECCS-1542205), and the Initiative for Sustainability and Energy (ISEN) at Northwestern University. We kindly thank Prof. H. Liu and Dr. Y. Zhang from Department of Electronic and Electrical Engineering at University College London for providing the GaAs nanowire sample. This work made use of the EPIC facility of Northwestern University's NUANCE Center, which has received support from the Soft and Hybrid Nanotechnology Experimental (SHyNE) Resource (NSF ECCS-1542205); the MRSEC program (NSF DMR-1121262) at the Materials Research Center; the International Institute for Nanotechnology (IIN); the Keck Foundation; and the State of Illinois through the IIN. We acknowledge Dr. Y. Xu and Dr. J. Wu of the NUANCE Center for assistance with TEM imaging of GaAs nanowires and for helpful discussions.

REFERENCES

- (1) Sun, Y.; Thompson, S.; Nishida, T. Physics of Strain Effects in Semiconductors and Metal-Oxide-Semiconductor Field-Effect Transistors. *J. Appl. Phys.* **2007**, *101*, 104503.
- (2) Ge, C. H.; Lin, C. C.; Ko, C. H.; Huang, C. C.; Huang, Y. C.; Chan, B. W.; Perng, B. C.; Sheu, C. C.; Tsai, P. Y.; Yao, L. G. In *Process-strained Si (PSS) CMOS Technology Featuring 3D Strain Engineering*; IEEE: Washington, DC, 2003; pp 3–7.
- (3) Conesa-Boj, S.; Hauge, H. I. T.; Verheijen, M. A.; Assali, S.; Li, A.; Bakkers, E.; Fontcuberta i Morral, A. Cracking the Si Shell Growth in Hexagonal GaP-Si Core-Shell Nanowires. *Nano Lett.* **2015**, *15*, 2974–2979.
- (4) Zanato, D.; Gokden, S.; Balkan, N.; Ridley, B. K.; Schaff, W. J. The Effect of Interface-Roughness and Dislocation Scattering on Low Temperature Mobility of 2D Electron Gas in GaN/AlGaN. Semicond. Sci. Technol. 2004, 19, 427.
- (5) Farvacque, J. L.; Douehan, J. C.; Von Alpen, U.; Gmelin, E. Screw-Dislocation-Induced Scattering Processes and Acceptor States in Te. *Phys. Status Solidi B* **1977**, *79*, 763–773.
- (6) Miyazawa, S.; Ishii, Y.; Ishida, S.; Nanishi, Y. Direct Observation of Dislocation Effects on Threshold Voltage of a GaAs Field-Effect Transistor. *Appl. Phys. Lett.* **1983**, 43, 853–855.
- (7) Siegelin, F.; Stuffer, A. Dislocation Related Leakage in Advanced CMOS devices. Proceedings from the 31st International Symposium for Testing and Failure Analysis, San Jose, CA, November 6–10, 2005; ASM International: Materials Park, OH, 2005; pp 59–63.
- (8) Lieber, C. M.; Wang, Z. L. Functional Nanowires. MRS Bull. **2007**, 32, 99–108.
- (9) Park, H. S.; Cai, W.; Espinosa, H. D.; Huang, H. Mechanics of Crystalline Nanowires. MRS Bull. 2009, 34, 178–183.
- (10) Roos, B.; Kapelle, B.; Richter, G.; Volkert, C. A. Surface Dislocation Nucleation Controlled Deformation of Au Nanowires. *Appl. Phys. Lett.* **2014**, *105*, 201908.
- (11) Stan, G.; Krylyuk, S.; Davydov, A. V.; Levin, I.; Cook, R. F. Ultimate Bending Strength of Si Nanowires. *Nano Lett.* **2012**, *12*, 2599–2604.
- (12) Hoffmann, S.; Utke, I.; Moser, B.; Michler, J.; Christiansen, S. H.; Schmidt, V.; Senz, S.; Werner, P.; Gösele, U.; Ballif, C. Measurement of the Bending Strength of Vapor-Liquid-Solid Grown Silicon Nanowires. *Nano Lett.* **2006**, *6*, 622–625.
- (13) Han, X.; Zheng, K.; Zhang, Y.; Zhang, X.; Zhang, Z.; Wang, Z. L. Low-Temperature *In Situ* Large-Strain Plasticity of Silicon Nanowires. *Adv. Mater.* **2007**, *19*, 2112–2118.
- (14) Zhang, H.; Tersoff, J.; Xu, S.; Chen, H.; Zhang, Q.; Zhang, K.; Yang, Y.; Lee, C.-S.; Tu, K.-N.; Li, J.; et al. Approaching the Ideal Elastic Strain Limit in Silicon Nanowires. *Sci. Adv.* **2016**, *2*, No. e1501382.
- (15) Wang, Y. B.; Wang, L. F.; Joyce, H. J.; Gao, Q.; Liao, X. Z.; Mai, Y. W.; Tan, H. H.; Zou, J.; Ringer, S. P.; Gao, H. J.; et al. Super

Deformability and Young's Modulus of GaAs Nanowires. *Adv. Mater.* **2011**, 23, 1356–1360.

- (16) Zheng, K.; Han, X.; Wang, L.; Zhang, Y.; Yue, Y.; Qin, Y.; Zhang, X.; Zhang, Z. Atomic Mechanisms Governing the Elastic Limit and the Incipient Plasticity of Bending Si Nanowires. *Nano Lett.* **2009**, 9, 2471–2476.
- (17) Chen, L. Y.; He, M.-r.; Shin, J.; Richter, G.; Gianola, D. S. Measuring Surface Dislocation Nucleation in Eefect-Scarce Nanostructures. *Nat. Mater.* **2015**, *14*, 707–713.
- (18) Brown, J. J.; Baca, A. I.; Bertness, K. A.; Dikin, D. A.; Ruoff, R. S.; Bright, V. M. Tensile Measurement of Single Crystal Gallium Nitride Nanowires on MEMS Test Stages. *Sens. Actuators, A* **2011**, *166*, 177–186.
- (19) Cheng, G.; Miao, C.; Qin, Q.; Li, J.; Xu, F.; Haftbaradaran, H.; Dickey, E. C.; Gao, H.; Zhu, Y. Large Anelasticity and Associated Energy Dissipation in Single-Crystalline Nanowires. *Nat. Nanotechnol.* **2015**, *10*, 687.
- (20) Dai, S.; Zhao, J.; Xie, L.; Cai, Y.; Wang, N.; Zhu, J. Electron-Beam-Induced Elastic—Plastic Transition in Si Nanowires. *Nano Lett.* **2012**, *12*, 2379—2385.
- (21) Wang, L.; Kong, D.; Xin, T.; Shu, X.; Zheng, K.; Xiao, L.; Sha, X.; Lu, Y.; Zhang, Z.; Han, X.; et al. Deformation Mechanisms of Bent Si Nanowires Governed by the Sign and Magnitude of Strain. *Appl. Phys. Lett.* **2016**, *108*, 151903.
- (22) Cahn, R. W. Recrystallization of Single Crystals after Plastic Bending. J. I. Met. 1949, 76, 121.
- (23) Hibbard, W. R., Jr; Dunn, C. G. A Study of < 112> Edge Dislocations in Bent Silicon-Iron Single Crystals. *Acta Metall.* **1956**, *4*, 306–315.
- (24) Gilman, J. J. Structure and Polygonization of Bent Zinc Monocrystals. *Acta Metall.* **1955**, *3*, 277–288.
- (25) Wolfe, C. M.; Nuese, C. J.; Holonyak, N., Jr Growth and Dislocation Structure of Single-Crystal Ga (As1 x Px). *J. Appl. Phys.* **1965**, *36*, 3790–3801.
- (26) Patel, J. R. Arrangements of Dislocations in Plastically Bent Silicon Crystals. *J. Appl. Phys.* **1958**, 29, 170–176.
- (27) Amelinckx, S. Etchpits and Dislocations along Grain Boundaries, Sliplines and Polygonization Walls. *Acta Metall.* **1954**, 2, 848–853.
- (28) Wang, L.; Kong, D.; Zhang, Y.; Xiao, L.; Lu, Y.; Chen, Z.; Zhang, Z.; Zou, J.; Zhu, T.; Han, X. Mechanically Driven Grain Boundary Formation in Nickel Nanowires. *ACS Nano* **2017**, *11*, 12500–12508.
- (29) Sun, Z.; Seidman, D. N.; Lauhon, L. J. Nanowire Kinking Modulates Doping Profiles by Reshaping the Liquid–Solid Growth Interface. *Nano Lett.* **2017**, *17*, 4518–4525.
- (30) John, C. S. The Brittle-to-Ductile Transition in Pre-Cleaved Silicon Single Crystals. *Philos. Mag.* **1975**, 32, 1193–1212.
- (31) De Wolf, I.; Maes, H. E.; Jones, S. K. Stress Measurements in Silicon Devices through Raman Spectroscopy: Bridging the Gap Between Theory and Experiment. J. Appl. Phys. 1996, 79, 7148–7156.
- (32) Hibbard, W. R.; Dunn, C. G. A Study of < 112> Edge Dislocations in Bent Silicon-Iron Single Crystals. *Acta Metall.* **1956**, *4*, 306–315.
- (33) Allen, J. E.; Hemesath, E. R.; Perea, D. E.; Lensch-Falk, J. L.; Li, Z. Y.; Yin, F.; Gass, M. H.; Wang, P.; Bleloch, A. L.; Palmer, R. E.; et al. High-Resolution Detection of Au Catalyst Atoms in Si Nanowires. *Nat. Nanotechnol.* **2008**, *3*, 168.
- (34) Hemesath, E. R.; Schreiber, D. K.; Gulsoy, E. B.; Kisielowski, C. F.; Petford-Long, A. K.; Voorhees, P. W.; Lauhon, L. J. Catalyst Incorporation at Defects during Nanowire Growth. *Nano Lett.* **2012**, *12*, 167–171.
- (35) Cottrell, A. H.; Bilby, B. A. Dislocation Theory of Yielding and Strain Ageing of Iron. *Proc. Phys. Soc., London, Sect. A* **1949**, *62*, 49.
- (36) Fahey, P. M.; Griffin, P. B.; Plummer, J. D. Point Defects and Dopant Diffusion in Silicon. *Rev. Mod. Phys.* **1989**, *61*, 289.
- (37) Ono, K.; Kino, T. Migration Energy of Mono-Vacancy in Aluminum at High Temperature. J. Phys. Soc. Jpn. 1978, 44, 875–881.

- (38) Seidman, D. N.; Balluffi, R. W. Sources of Thermally Generated Vacancies in Single-Crystal and Polycrystalline Gold. *Phys. Rev.* **1965**, 139, A1824.
- (39) Vogel, F. L., Jr Dislocations in Polygonized Germanium. *Acta Metall.* 1955, 3, 95–96.
- (40) Vogel, F. L., Jr On the Orientation Effect in the Polygonization of Bent Silicon Crystals. *Acta Metall.* **1958**, *6*, 532–534.
- (41) Zhu, T.; Li, J.; Samanta, A.; Leach, A.; Gall, K. Temperature and Strain-Rate Dependence of Surface Dislocation Nucleation. *Phys. Rev. Lett.* **2008**, *100*, 025502.
- (42) Chachamovitz, D.; Mordehai, D. The Stress-Dependent Activation Parameters for Dislocation Nucleation in Molybdenum Nanoparticles. *Sci. Rep.* **2018**, *8*, 3915.
- (43) Eymery, J.; Buttard, D.; Fournel, F.; Moriceau, H.; Baumbach, G. T.; Lübbert, D. Dislocation Strain Field in Ultrathin Bonded Silicon Wafers Studied by Grazing Incidence X-ray Diffraction. *Phys. Rev. B: Condens. Matter Mater. Phys.* **2002**, *65*, 165337.
- (44) Cai, W.; Nix, W. D. Imperfections in Crystalline Solids; Cambridge University Press: Cambridge, 2016.
- (45) Anderson, P. M.; Hirth, J. P.; Lothe, J. Theory of Dislocations; Cambridge University Press: Cambridge, 2017.
- (46) Kabir, M.; Lau, T. T.; Rodney, D.; Yip, S.; Van Vliet, K. J. Predicting Dislocation Climb and Creep from Explicit Atomistic Details. *Phys. Rev. Lett.* **2010**, *105*, 095501.
- (47) Gilman, J. J.; Johnston, W. G. Observations of Dislocation Glide and Climb in Lithium Fluoride Crystals. *J. Appl. Phys.* **1956**, *27*, 1018–1022.
- (48) Sadigh, B.; Lenosky, T. J.; Caturla, M.-J.; Quong, A. A.; Benedict, L. X.; Diaz de la Rubia, T.; Giles, M. M.; Foad, M.; Spataru, C. D.; Louie, S. G. Large Enhancement of Boron Solubility in Silicon due to Biaxial Stress. *Appl. Phys. Lett.* **2002**, *80*, 4738–4740.
- (49) Zhu, J.; Liu, F.; Stringfellow, G. B.; Wei, S.-H. Strain-Enhanced Doping in Semiconductors: Effects of Dopant Size and Charge State. *Phys. Rev. Lett.* **2010**, *105*, 195503.
- (50) Sun, Z.; Hazut, O.; Yerushalmi, R.; Lauhon, L. J.; Seidman, D. N. Criteria and Considerations for Preparing Atom-Probe Tomography Specimens of Nanomaterials Utilizing an Encapsulation Methodology. *Ultramicroscopy* **2018**, *184*, 225–233.
- (51) Sun, Z.; Hazut, O.; Huang, B.-C.; Chiu, Y.-P.; Chang, C.-S.; Yerushalmi, R.; Lauhon, L. J.; Seidman, D. N. Dopant Diffusion and Activation in Silicon Nanowires Fabricated by *Ex Situ* Doping: A Correlative Study *via* Atom-Probe Tomography and Scanning Tunneling Spectroscopy. *Nano Lett.* **2016**, *16*, 4490–4500.
- (52) Wang, S.; Pirouz, P. Mechanical Properties of Undoped GaAs. II: The Brittle-to-Ductile Transition Temperature. *Acta Mater.* **2007**, 55, 5515–5525.
- (53) Zhou, Z. Y.; Zheng, C. X.; Tang, W. X.; Jesson, D. E.; Tersoff, J. Congruent Evaporation Temperature of GaAs(001) Controlled by As Flux. *Appl. Phys. Lett.* **2010**, *97*, 121912.
- (54) Foxon, C. T.; Harvey, J. A.; Joyce, B. A. The Evaporation of GaAs under Equilibrium and Non-equilibrium Conditions using a Modulated Beam Technique. *J. Phys. Chem. Solids* **1973**, *34*, 1693–1701
- (55) Goldstein, B.; Szostak, D. J.; Ban, V. S. Langmuir evaporation from the (100), (111A), and (111B) faces of GaAs. *Surf. Sci.* **1976**, 57, 733–740.
- (56) Weertman, J. X. In *Dislocation Based Fracture Mechanics*; World Scientific Publishing Company: Singapore, 1996.